





Nanophotonic Approach to Study Excited-State Dynamics in Semiconductor Nanocrystals

Journal Article

Author(s):

Cocina, Ario; Brechbühler, Raphael ; Vonk, Sander J.W.; Cui, Jian; Rossinelli, Aurelio ; Rojo Sanz, Maria del Hena ; Rabouw, Freddy T.; Norris, David J. 

Publication date:

2022-05-12

Permanent link:

<https://doi.org/10.3929/ethz-b-000552125>

Rights / license:

[In Copyright - Non-Commercial Use Permitted](#)

Originally published in:

The Journal of Physical Chemistry Letters 13(18), <https://doi.org/10.1021/acs.jpcclett.2c00599>

Funding acknowledgement:

339905 - Quantum-Dot Plasmonics and Spasers (EC)
165559 - Optical Strong Coupling in Colloidal Quantum Dots (SNF)

A Nanophotonic Approach to Study Excited-State Dynamics in Semiconductor Nanocrystals

Ario Cocina,¹ Raphael Brechbühler,^{1,2} Sander J. W. Vonk,³ Jian Cui,^{1,4} Aurelio A. Rossinelli,¹ Henar Rojo,¹ Freddy T. Rabouw,^{1,3} and David J. Norris^{,1}*

¹Optical Materials Engineering Laboratory, Department of Mechanical and Process Engineering, ETH Zurich, 8092 Zurich, Switzerland

²Laboratory for Air Pollution and Environmental Technology, Empa, 8600 Dübendorf, Switzerland

³Debye Institute for Nanomaterials Science, Utrecht University, 3584 CC Utrecht, The Netherlands

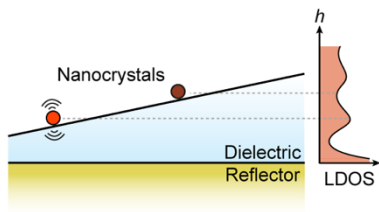
⁴Helmholtz Pioneer Campus, Helmholtz Zentrum München, 85764 Neuherberg, Germany

*Email: dnorris@ethz.ch

ABSTRACT. In semiconductor nanocrystals, excited electrons relax through multiple radiative and nonradiative pathways. This complexity complicates characterization of their decay processes with standard time- and temperature-dependent photoluminescence studies. Here, we exploit a simple nanophotonic approach to augment such measurements and address open questions related to nanocrystal emission. We place nanocrystals at different distances from a gold reflector to affect radiative rates through variations in the local density of optical states. We apply this approach to spherical CdSe-based nanocrystals to probe the radiative efficiency and polarization properties of the lowest dark and bright excitons by analyzing temperature-dependent emission dynamics. For CdSe-based nanoplatelets, we identify the charge-carrier trapping mechanism responsible for strongly delayed emission. Our method, when combined with careful modeling of the influence of the nanophotonic environment on the relaxation dynamics, offers a versatile strategy to disentangle the complex excited-state decay pathways present in fluorescent nanocrystals as well as other emitters.

KEYWORDS. colloidal quantum dots, photonic density of states, Purcell effect, Drexhage experiment, delayed emission

TOC GRAPHIC



Semiconductor nanocrystals (NCs) offer unique optical properties for applications due to their dimensions. This has driven the production of high-quality particles of different materials^{1–3} with control over size,¹ shape,^{4,5} stability,^{6,7} and fluorescence efficiency.^{7,8} To optimize performance, their photophysics has also been heavily investigated. In particular, time-resolved spectroscopy has been utilized.^{9–11} After excitation of a NC with a laser pulse, the photogenerated electron–hole pair (exciton) relaxes. This process can be monitored by measuring photoluminescence decay traces or transient absorption spectra. Indeed, such techniques have revealed the primary decay mechanisms in NCs, such as direct radiative and nonradiative recombination,¹² Auger recombination,^{9,13} charge-carrier trapping,^{14–21} and energy transfer.^{22,23} However, because multiple energy levels are typically involved, the interpretation of experiments is often challenging.

A common strategy to disentangle the complex excited-state dynamics of NCs has been to vary experimental parameters that modify the interplay between different relaxation processes. Examples include temperature to alter thermal populations,^{24–26} magnetic fields to mix electronic levels,^{24,27,28} and excitation power to affect carrier density (which influences Auger recombination).¹³ However, an important additional parameter has not yet been fully exploited—the local density of optical states (LDOS). In other words, the local electromagnetic environment can be varied. Photon-emission rates depend²⁹ on LDOS,^{30–39} while nonradiative relaxation remains unaffected. Pioneered by Drexhage,³⁰ modification of LDOS has successfully quantified the competition between radiative and nonradiative recombination (i.e., the quantum yield) in various emitters by measuring their excited-state decay at controlled distances from a reflector.^{35,36,38} Furthermore, insights into the interplay of radiative recombination and spin-flip transitions³⁹ or energy transfer^{34,37} were gained. If LDOS changes were similarly applied to study the complex dynamics of NCs, this could potentially clarify

open questions. To follow this approach, detailed modeling and in-depth analyses of the effects of LDOS beyond previous studies would be required.

Here, we pursue LDOS as a useful parameter to investigate NCs. We systematically change the photonic environment of two types of NCs and study the effect on their excited-state dynamics. We develop a cryostat-compatible implementation of Drexhage's method by depositing NCs on a thin, wedge-shaped layer of alumina (Al_2O_3), which covers a planar Au film. The ramp in alumina thickness places NCs at different distances from the Au reflector. Through a detailed analysis of the NC emission on such structures, we extract the influence of LDOS on the dynamics. Applied to spherical CdSe-based NCs (known as colloidal quantum dots, cQDs), we examine the dominant radiative and nonradiative recombination mechanisms at cryogenic temperatures, which are controlled by the two lowest exciton fine-structure states.^{40,41} For CdSe-based nanoplatelets (NPLs), we determine the mechanism of reversible charge-carrier trapping, which strongly affects the overall decay dynamics.¹⁹ Thus, our results provide insights into the excited-state processes of important classes of NCs. More generally, this approach can help investigate relaxation pathways in other emitters.

Figure 1 introduces the structures we use to control LDOS. A planar Au-coated substrate was gradually exposed to Al_2O_3 flux by moving the substrate relative to a shadowing mask in a reactive sputterer (Figure 1a). This procedure yielded a layer of Al_2O_3 with a linearly varying thickness of 0–800 nm over 7 mm (Figure 1b; section S1 in the Supporting Information). CdSe/ZnS core/shell cQDs or CdSe/ $\text{Cd}_x\text{Zn}_{1-x}\text{S}$ core/shell NPLs were then deposited on this wedge by spin-coating from dilute dispersions, resulting in sparse films (Figure 1c and Figure S1 in the Supporting Information). On such a structure, the NCs experience an LDOS that depends on their position. Specifically, Figure 1d shows how the LDOS, $\rho(h)$, averaged over all optical polarizations, depends on the local wedge thickness h . The radiative rate k_{rad} of an emitter, e.g., a NC, is given by $k_{\text{rad}}(h) = k_{\text{rad},0} \rho_r(h)$, where $k_{\text{rad},0}$ is the radiative rate of the

emitter in vacuum, and $\rho_r(h) = \rho(h)/\rho_0$ is the LDOS relative to the LDOS in vacuum, ρ_0 . The surface density of NCs on our structures is $\sim 0.5\text{--}1$ emitters/ μm^2 . Hence, below we probe $\sim 630\text{--}1260$ NCs within our illumination spot ($20\ \mu\text{m}$ radius). All NCs within this spot experience nearly identical LDOS, as h varies by only 5 nm (see Figure 1d).

We first use such structures to investigate the relaxation of CdSe/ZnS core/shell cQDs (2.3-nm cores with 4-monolayer-thick shells) at cryogenic temperatures. Despite decades of investigation,^{24,42} the low-temperature photoluminescence (PL) of CdSe-based cQDs is still discussed, fueled most recently by a proposal for the recombination mechanism of the dark exciton.^{40,41} The PL of our CdSe/ZnS cQDs at 3.2 K (Figure 2a) presents a two-component decay, typical of such systems. This has been explained in terms of emission from two energy levels in thermal equilibrium: an upper bright state (B) and a lower dark state (D), separated by an energy splitting ΔE (Figure 2b).^{24–26} The fast component has been attributed to an initial B population that relaxes to D nonradiatively on a ns time scale, while the long component results from recombination of both B and D in thermal equilibrium. (In our measurements at cryogenic temperatures, the fast decay comes mainly from Al_2O_3 background fluorescence. This, however, does not affect the long component from the cQDs; see section S3 in the Supporting Information). When the thermal energy is much smaller than ΔE , the slow decay is caused mostly by D, which recombines slowly.^{27,43} As the temperature T is increased, the thermal population of fast-emitting B is enhanced, causing the long component to shorten and grow in relative amplitude (Figure 2a). Hence, the long component and its temperature dependence carry information about the decay processes from both dark and bright exciton states (section S5 in the Supporting Information).

To probe the radiative content of the long component and its temperature evolution, we measured the decay for different h over a range of temperatures (see Figures S3 and S4 in the Supporting Information). Figure 2c shows the fitted temperature- and LDOS-dependent

lifetimes. The long component becomes 6 times faster as we increase T from 3.2 to 37 K, consistent with increasing the thermal occupation of B. At any T , the lifetime value shows an oscillation of $\pm 25\%$ around the mean as we increase h . This indicates a strong LDOS dependency of the excited-state lifetime and thus a dominant role of radiative (versus nonradiative) recombination. Interestingly, we observe a slight difference between the lifetime oscillations as a function of h at 3.2 K, where emission is mainly from D, compared to 37 K, where it is mainly from B. The peaks of the oscillations are found at slightly smaller h at 3.2 K versus 37 K (Figure 2d). This subtle difference can potentially provide information about the emission of D, e.g., the polarization of D with the respect to B.

In CdSe-based cQDs, B is known to emit as a two-dimensional electric dipole.^{27,44} The orange line in Figure 2d shows the calculated lifetime oscillation for an ensemble of randomly oriented two-dimensional dipoles (section S5 in the Supporting Information). Although the emission polarization of D is still debated, it could involve a two-dimensional dipole lying on a plane *perpendicular* to the c -axis of the cQD and/or a one-dimensional dipole *parallel* to the c -axis, depending on the process that mediates its activation.⁴³ A pure one-dimensional dipole for D is not consistent with our experiments, as randomly oriented one-dimensional dipoles would show lifetime oscillations that peak at larger h than two-dimensional dipoles (compare dashed and orange lines in Figure 2d). Rather, the lifetime oscillations at slightly smaller h appear to be more consistent with a three-dimensional dipole (blue line in Figure 2d).

We can rationalize these results by considering the proposal in refs 40 and 41 in which the recombination of D is mediated by phonons at very low temperatures and spins from dangling bonds at slightly higher temperatures,^{40,41} yielding one-dimensional- and two-dimensional-dipole polarizations, respectively, each orthogonal to each other. Indeed, if we include the two recombination mechanisms in our model, we can produce an effective three-dimensional-dipole polarization at intermediate temperatures (section S5 in the Supporting Information).

To extract quantitative information, we globally fit the lifetime values at all temperatures and distances to such a model, sketched in Figure 2b. The fitted curves are the solid lines in Figure 2c. The fit yields the radiative efficiencies in vacuum for B and D (η_B^0 and η_D^0), as well as ΔE , the vacuum radiative rates, and other model parameters (see Table S1 in the Supporting Information). The extracted values for η_B^0 and η_D^0 are large ($\sim 100\%$), consistent with assumptions used in previous studies of CdSe-based cQDs.^{25,26} A large η_D^0 implies the absence of nonradiative recombination channels from the dark state. This distinguishes our cQDs from other NCs where emission from D was reported to be inefficient, including epitaxial QDs³⁹ and perovskite NCs.^{28,45}

We now turn to CdSe-based NPLs. Because these NCs have a rectangular, quasi-2D shape with a precise, atomic-scale thickness, they exhibit narrow emission features that are useful for applications.⁴⁶ However, temporary trapping of charge carriers has been shown to slow radiative recombination.^{19,47} Indeed, the PL decay curve of our NPLs has a characteristic power-law tail from 50 ns to 1 μ s (Figure 3a). This tail is due to trapping of photogenerated charge carriers followed by detrapping and radiative recombination.¹⁹ The broadly distributed *detrapping* rates are evident from the long decay, but the *trapping* process is difficult to characterize with time-resolved PL experiments. Indeed, while pump–probe methods can be used to characterize all trapping events,^{48,49} PL-based methods struggle because the trapping time scales overlap with both prompt recombination and the fastest detrapping processes. Consequently, the same PL decay can be explained with two different trapping models:^{14,50} cold-carrier trapping or hot-carrier trapping (Figure 3c). In cold trapping, the charge carriers cool to the lowest excited state before trapping, while in hot trapping, they trap from a higher excited state. To determine which model is correct, we examine the LDOS dependence of the delayed emission.¹⁴ We perform our measurements at room temperature, where delayed emission can potentially affect emission saturation in light-emitting NPL devices. The alumina

background fluorescence is negligible at the NPL emission wavelength (see section S3 in the Supporting Information).

Figure 3a shows the PL decay of our NPLs (4-monolayer-thick CdSe cores with 2-nm-thick $\text{Cd}_x\text{Zn}_{1-x}\text{S}$ shells⁵¹) at two different h with high (blue) and low (red) LDOS. The two curves show different behavior over the first 50 ns, while afterwards the delayed emission shows the same power-law slope. To compare the distributed dynamics between different measurements, we describe the slope of the PL decay curve, which depends on the time t after photoexcitation, in terms of an “instantaneous lifetime,”¹⁹ $\tau_{\text{inst}}(t) = -I(t) / I'(t)$, where $I(t)$ is the PL decay curve and $I'(t)$ its time derivative. Comparison of $\tau_{\text{inst}}(t)$ for the measurements at high and low LDOS (Figure 3b) confirms that the early-time dynamics is affected by the photonic environment, while the delayed-emission dynamics is not. Figure 3d shows the instantaneous lifetime of our NPLs as a function of t for a range of h . At each time, the instantaneous lifetime values at different heights are normalized to their mean. Figure 3d is divided into two time regions, displaying qualitatively different LDOS sensitivity. The region $t < 50$ ns shows oscillations, which fade for $t > 50$ ns. Figure 3e,f shows vertical cuts through Figure 3d, highlighting the oscillations for times $t = 20\text{--}30$ ns and the LDOS-independence for $t = 200\text{--}300$ ns, respectively.

These observations make intuitive sense. The early-time decay is (in part) due to radiative recombination, leading to LDOS dependence. Radiative recombination is presumably in competition with nonradiative recombination and, in the scenario of cold trapping, charge-carrier trapping. At longer times, charge-carrier detrapping is presumably the rate-limiting step (i.e., the slowest step in the delayed-emission process). Detrapping is expected to be LDOS independent. This explanation holds both for the hot-trapping and cold-trapping models with distributed detrapping rates. (For cold trapping with a single detrapping rate, the LDOS dependence at long delay times would remain; see section S6 in the Supporting Information.)

Indeed, a global fit of the data (Figure 3d) produces a good match, independent of whether we assume cold or hot trapping (compare blue and red lines in Figure 3e,f). Thus, the instantaneous-lifetime analysis cannot provide enough information to discern the trapping mechanism.

However, we can distinguish between hot and cold trapping if we consider the delayed-emission *intensity* as a function of LDOS. Figure 3g presents our experimental data as a color map of $I(t, h)/I_{\text{tot}}(h)$. $I(t, h)$ is the PL decay curve at distance h and $I_{\text{tot}}(h) = \int_0^{\infty} I(t, h) dt$ is its time-integrated intensity. With increasing t , we observe an inversion of the LDOS-associated oscillations. Namely, for $t = 5\text{--}10$ ns (Figure 3h) the intensity ratio $I(t, h)/I_{\text{tot}}(h)$ shows dips at $h = 200, 425,$ and 650 nm, while at $t = 200\text{--}300$ ns (Figure 3i) it peaks at these values. This is a strong indication of cold trapping. At $h = 200, 425,$ and 650 nm, where the LDOS is minimized, the initial excited electronic state exhibits a slower radiative decay. Consequently, the intensity of prompt emission ($t < 50$ ns) is reduced, and the probability of trapping, which in cold trapping is determined by the competition between trapping and emission, is enhanced. This leads to more delayed emission at later times ($t > 50$ ns). The situation is exactly the opposite at $h = 90, 300, 525,$ and 750 nm, where the LDOS peaks. Emission at early times is enhanced, decreasing delayed emission. This opposite effect of LDOS on the early and delayed emission causes the inversion of the oscillations.

Hot trapping will not produce such an inversion. In this case, trapping competes with hot-carrier cooling rather than radiative recombination. Thus, trapping does not compete with an LDOS-dependent process (see section S6 in the Supporting Information). To quantify this explanation, we calculated the expected results for hot and cold trapping in Figure 3h,i, using only parameters obtained from fits to the instantaneous-lifetime data (Figure 3e,f). The cold-trapping model (blue lines in Figure 3h,i) reproduces the experiment, while the hot-trapping model (red lines) does not. We conclude that trapping in our NPLs occurs from the lowest

excited state. Further, we extract a trapping rate of $1/121 \text{ ns}^{-1}$, which competes with a vacuum radiative recombination rate of $1/74 \text{ ns}^{-1}$ and a nonradiative recombination rate of $1/41 \text{ ns}^{-1}$.

In summary, we have exploited the nanophotonic environment to address open questions related to excited-state dynamics in CdSe-based NCs. By placing NCs on a simple alumina-on-gold structure, their emission is affected by changes in LDOS. Using this effect, we determined that the two lowest-energy electronic states in CdSe/ZnS core/shell cQDs have high radiative efficiency. Our results also suggest that the lowest dark state emits as an effective three-dimensional isotropic dipole. Second, we obtained direct evidence for the charge-carrier-trapping mechanism that causes delayed emission in CdSe/CdZnS core/shell NPLs. Charge carriers are trapped from the lowest excited state (cold trapping) and return to this state by detrapping over a wide range of time scales. In addition to revealing further insights into NC photophysics, we have demonstrated that LDOS provides another experimental parameter, like temperature or magnetic field, to clarify relaxation processes in complex emitters.

EXPERIMENTAL METHODS

A detailed description of the experimental methods is provided in the Supporting Information.

ASSOCIATED CONTENT

Supporting Information

The Supporting Information is available free of charge.

Additional experimental details, raw data, and modeling, including sample fabrication (section S1), optical measurements and sample characterization (section S2), characterization of the background fluorescence (section S3), decay-fitting strategies (section S4), modeling of the cQD emission (section S5), modeling of the NPL emission (section S6), calculations of the average number of excitons per NC (section S7),

supplementary figures and tables (section S8), and supplementary references (section S9)
(pdf)

AUTHOR INFORMATION

ORCID

Ario Cocina: 0000-0003-1560-5849

Raphael Brechbühler: 0000-0001-7498-9729

Sander J. W. Vonk: 0000-0002-4650-9473

Jian Cui: 0000-0002-2394-3357

Aurelio A. Rossinelli: 0000-0001-6930-4190

Henar Rojo: 0000-0003-1543-6264

Freddy T. Rabouw: 0000-0002-4775-0859

David J. Norris: 0000-0002-3765-0678

Notes

The authors declare no competing financial interests.

ACKNOWLEDGMENT

This work was supported by the European Research Council under the European Union's Seventh Framework Program (FP/2007-2013) ERC Grant Agreement Nr. 339905 (QuaDoPS Advanced Grant) and by the Swiss National Science Foundation (SNSF) under grant no. 200021_165559. F.T.R. acknowledges support from the Netherlands Organisation for Scientific Research (Gravitation Program “Multiscale Catalytic Energy Conversion,” Veni-722.017.002, OCENW.KLEIN.008). The authors thank the Cleanroom Operations Team of the Binnig and Rohrer Nanotechnology Center (BRNC) and S. Meyer for help and support with fabrication. The authors also thank R. Keitel for stimulating discussions.

REFERENCES

- (1) Murray, C. B.; Norris, D. J.; Bawendi, M. G. Synthesis and Characterization of Nearly Monodisperse CdE (E = S, Se, Te) Semiconductor Nanocrystallites. *J. Am. Chem. Soc.* **1993**, *115*, 8706–8715.
- (2) Mičić, O. I.; Curtis, C. J.; Jones, K. M.; Sprague, J. R.; Nozik, A. J. Synthesis and Characterization of InP Quantum Dots. *J. Phys. Chem.* **1994**, *98*, 4966–4969.
- (3) Protesescu, L.; Yakunin, S.; Bodnarchuk, M. I.; Krieg, F.; Caputo, R.; Hendon, C. H.; Yang, R. X.; Walsh, A.; Kovalenko, M. V. Nanocrystals of Cesium Lead Halide Perovskites (CsPbX₃, X = Cl, Br, and I): Novel Optoelectronic Materials Showing Bright Emission with Wide Color Gamut. *Nano Lett.* **2015**, *15*, 3692–3696.
- (4) Ithurria, S.; Dubertret, B. Quasi 2D Colloidal CdSe Platelets with Thicknesses Controlled at the Atomic Level. *J. Am. Chem. Soc.* **2008**, *130*, 16504–16505.
- (5) Peng, X.; Manna, L.; Yang, W.; Wickham, J.; Scher, E.; Kadavanich, A.; Alivisatos, A. P. Shape Control of CdSe Nanocrystals. *Nature* **2000**, *404*, 59–61.
- (6) Hines, M. A.; Guyot-Sionnest, P. Synthesis and Characterization of Strongly Luminescing ZnS-Capped CdSe Nanocrystals. *J. Phys. Chem.* **1996**, *100*, 468–471.
- (7) Chen, O.; Zhao, J.; Chauhan, V. P.; Cui, J.; Wong, C.; Harris, D. K.; Wei, H.; Han, H. S.; Fukumura, D.; Jain, R. K.; Bawendi, M. G. Compact High-Quality CdSe-CdS Core-Shell Nanocrystals with Narrow Emission Linewidths and Suppressed Blinking. *Nat. Mater.* **2013**, *12*, 445–451.
- (8) Chen, Y.; Vela, J.; Htoon, H.; Casson, J. L.; Werder, D. J.; Bussian, D. A.; Klimov, V. I.; Hollingsworth, J. A. “Giant” Multishell CdSe Nanocrystal Quantum Dots with Suppressed Blinking. *J. Am. Chem. Soc.* **2008**, *130*, 5026–5027.
- (9) Nirmal, M.; Dabbousi, B. O.; Bawendi, M. G.; Macklin, J. J.; Trautman, J. K.; Harris, T. D.; Brus, L. E. Fluorescence Intermittency in Single Cadmium Selenide Nanocrystals. *Nature* **1996**, *383*, 802–804.
- (10) Nirmal, M.; Murray, C. B.; Bawendi, M. G. Fluorescence-Line Narrowing in CdSe Quantum Dots: Surface Localization of the Photogenerated Exciton. *Phys. Rev. B* **1994**, *50*, 2293–2300.
- (11) Fisher, B. R.; Eisler, H. J.; Stott, N. E.; Bawendi, M. G. Emission Intensity Dependence and Single-Exponential Behavior in Single Colloidal Quantum Dot Fluorescence Lifetimes. *J. Phys. Chem. B* **2004**, *108*, 143–148.
- (12) Yuan, G.; Gómez, D. E.; Kirkwood, N.; Boldt, K.; Mulvaney, P. Two Mechanisms Determine Quantum Dot Blinking. *ACS Nano* **2018**, *12*, 3397–3405.
- (13) Park, Y. S.; Bae, W. K.; Baker, T.; Lim, J.; Klimov, V. I. Effect of Auger Recombination on Lasing in Heterostructured Quantum Dots with Engineered Core/Shell Interfaces. *Nano Lett.* **2015**, *15*, 7319–7328.
- (14) Rabouw, F. T.; Kamp, M.; Van Dijk-Moes, R. J. A.; Gamelin, D. R.; Koenderink, A. F.; Meijerink, A.; Vanmaekelbergh, D. Delayed Exciton Emission and Its Relation to Blinking in CdSe Quantum Dots. *Nano Lett.* **2015**, *15*, 7718–7725.

- (15) Whitham, P. J.; Knowles, K. E.; Reid, P. J.; Gamelin, D. R. Photoluminescence Blinking and Reversible Electron Trapping in Copper-Doped CdSe Nanocrystals. *Nano Lett.* **2015**, *15*, 4045–4051.
- (16) Whitham, P. J.; Marchioro, A.; Knowles, K. E.; Kilburn, T. B.; Reid, P. J.; Gamelin, D. R. Single-Particle Photoluminescence Spectra, Blinking, and Delayed Luminescence of Colloidal CuInS₂ Nanocrystals. *J. Phys. Chem. C* **2016**, *120*, 17136–17142.
- (17) Marchioro, A.; Whitham, P. J.; Knowles, K. E.; Kilburn, T. B.; Reid, P. J.; Gamelin, D. R. Tunneling in the Delayed Luminescence of Colloidal CdSe, Cu⁺-Doped CdSe, and CuInS₂ Semiconductor Nanocrystals and Relationship to Blinking. *J. Phys. Chem. C* **2016**, *120*, 27040–27049.
- (18) Righetto, M.; Minotto, A.; Bozio, R. Bridging Energetics and Dynamics of Exciton Trapping in Core-Shell Quantum Dots. *J. Phys. Chem. C* **2017**, *121*, 896–902.
- (19) Rabouw, F. T.; Van Der Bok, J. C.; Spinicelli, P.; Mahler, B.; Nasilowski, M.; Pedetti, S.; Dubertret, B.; Vanmaekelbergh, D. Temporary Charge Carrier Separation Dominates the Photoluminescence Decay Dynamics of Colloidal CdSe Nanoplatelets. *Nano Lett.* **2016**, *16*, 2047–2053.
- (20) Becker, M. A.; Bernasconi, C.; Bodnarchuk, M. I.; Raino, G.; Kovalenko, M. V.; Norris, D. J.; Mahrt, R. F.; Stöferle, T. Unraveling the Origin of the Long Fluorescence Decay Component of Cesium Lead Halide Perovskite Nanocrystals. *ACS Nano* **2020**, *14*, 14939–14946.
- (21) Vonk, S. J. W.; Fridriksson, M. B.; Hinterding, S. O. M.; Mangnus, M. J. J.; Van Swieten, T. P.; Grozema, F. C.; Rabouw, F. T.; Van Der Stam, W. Trapping and Detrapping in Colloidal Perovskite Nanoplatelets: Elucidation and Prevention of Nonradiative Processes through Chemical Treatment. *J. Phys. Chem. C* **2020**, *124*, 8047–8054.
- (22) Kagan, C. R.; Murray, C. B.; Nirmal, M.; Bawendi, M. G. Electronic Energy Transfer in CdSe Quantum Dot Solids. *Phys. Rev. Lett.* **1996**, *76*, 1517–1520.
- (23) Prins, F.; Goodman, A. J.; Tisdale, W. A. Reduced Dielectric Screening and Enhanced Energy Transfer in Single- and Few-Layer MoS₂. *Nano Lett.* **2014**, *14*, 6087–6091.
- (24) Nirmal, M.; Norris, D. J.; Kuno, M.; Bawendi, M. G.; Efros, A. L.; Rosen, M. Observation of the “Dark Exciton” in CdSe Quantum Dots. *Phys. Rev. Lett.* **1995**, *75*, 3728–3731.
- (25) Labeau, O.; Tamarat, P.; Lounis, B. Temperature Dependence of the Luminescence Lifetime of Single CdSe/ZnS Quantum Dots. *Phys. Rev. Lett.* **2003**, *90*, 257404.
- (26) De Mello Donegá, C.; Bode, M.; Meijerink, A. Size- and Temperature-Dependence of Exciton Lifetimes in CdSe Quantum Dots. *Phys. Rev. B* **2006**, *74*, 085320.
- (27) Efros, A. L.; Rosen, M.; Kuno, M.; Nirmal, M.; Norris, D.; Bawendi, M. Band-Edge Exciton in Quantum Dots of Semiconductors with a Degenerate Valence Band: Dark and Bright Exciton States. *Phys. Rev. B* **1996**, *54*, 4843–4856.
- (28) Tamarat, P.; Bodnarchuk, M. I.; Trebbia, J. B.; Erni, R.; Kovalenko, M. V.; Even, J.; Lounis, B. The Ground Exciton State of Formamidinium Lead Bromide Perovskite

- Nanocrystals Is a Singlet Dark State. *Nat. Mater.* **2019**, *18*, 717–724.
- (29) Novotny, L.; Hecht, B. *Principles of Nano-Optics*; Cambridge University Press: Cambridge, 2012.
- (30) Drexhage, K. H. Influence of a Dielectric Interface on Fluorescence Decay Time. *J. Lumin.* **1970**, *1–2*, 693–701.
- (31) Brokmann, X.; Coolen, L.; Dahan, M.; Hermier, J. P. Measurement of the Radiative and Nonradiative Decay Rates of Single CdSe Nanocrystals through a Controlled Modification of Their Spontaneous Emission. *Phys. Rev. Lett.* **2004**, *93*, 107403.
- (32) Stobbe, S.; Johansen, J.; Kristensen, P. T.; Hvam, J. M.; Lodahl, P. Frequency Dependence of the Radiative Decay Rate of Excitons in Self-Assembled Quantum Dots: Experiment and Theory. *Phys. Rev. B* **2009**, *80*, 155307.
- (33) Leistikow, M. D.; Johansen, J.; Kettelarij, A. J.; Lodahl, P.; Vos, W. L. Size-Dependent Oscillator Strength and Quantum Efficiency of CdSe Quantum Dots Controlled via the Local Density of States. *Phys. Rev. B* **2009**, *79*, 045301.
- (34) Blum, C.; Zijlstra, N.; Lagendijk, A.; Wubs, M.; Mosk, A. P.; Subramaniam, V.; Vos, W. L. Nanophotonic Control of the Förster Resonance Energy Transfer Efficiency. *Phys. Rev. Lett.* **2012**, *109*, 203601.
- (35) Kwadrin, A.; Koenderink, A. F. Gray-Tone Lithography Implementation of Drexhage's Method for Calibrating Radiative and Nonradiative Decay Constants of Fluorophores. *J. Phys. Chem. C* **2012**, *116*, 16666–16673.
- (36) Lunnemann, P.; Rabouw, F. T.; Van Dijk-Moes, R. J. A.; Pietra, F.; Vanmaekelbergh, D.; Koenderink, A. F. Calibrating and Controlling the Quantum Efficiency Distribution of Inhomogeneously Broadened Quantum Rods by Using a Mirror Ball. *ACS Nano* **2013**, *7*, 5984–5992.
- (37) Senden, T.; Rabouw, F. T.; Meijerink, A. Photonic Effects on the Radiative Decay Rate and Luminescence Quantum Yield of Doped Nanocrystals. *ACS Nano* **2015**, *9*, 1801–1808.
- (38) Li, D.; Karaveli, S.; Cuff, S.; Li, W.; Zia, R. Probing the Combined Electromagnetic Local Density of Optical States with Quantum Emitters Supporting Strong Electric and Magnetic Transitions. *Phys. Rev. Lett.* **2018**, *121*, 227403.
- (39) Johansen, J.; Julsgaard, B.; Stobbe, S.; Hvam, J. M.; Lodahl, P. Probing Long-Lived Dark Excitons in Self-Assembled Quantum Dots. *Phys. Rev. B* **2010**, *81*, 081304.
- (40) Rodina, A.; Efros, A. L. Magnetic Properties of Nonmagnetic Nanostructures: Dangling Bond Magnetic Polaron in CdSe Nanocrystals. *Nano Lett.* **2015**, *15*, 4214–4222.
- (41) Biadala, L.; Shornikova, E. V.; Rodina, A. V.; Yakovlev, D. R.; Siebers, B.; Aubert, T.; Nasilowski, M.; Hens, Z.; Dubertret, B.; Efros, A. L.; Bayer, M. Magnetic Polaron on Dangling-Bond Spins in CdSe Colloidal Nanocrystals. *Nat. Nanotechnol.* **2017**, *12*, 569–574.
- (42) Bawendi, M. G.; Carroll, P. J.; Wilson, W. L.; Brus, L. E. Luminescence Properties of CdSe Quantum Crystallites: Resonance between Interior and Surface Localized States.

J. Chem. Phys. **1992**, *96*, 946–954.

- (43) Rodina, A. V.; Efros, A. L. Radiative Recombination from Dark Excitons in Nanocrystals: Activation Mechanisms and Polarization Properties. *Phys. Rev. B* **2016**, *93*, 155427.
- (44) Fernée, M. J.; Littleton, B. N.; Rubinsztein-Dunlop, H. Detection of Bright Trion States Using the Fine Structure Emission of Single CdSe/ZnS Colloidal Quantum Dots. *ACS Nano* **2009**, *3*, 3762–3768.
- (45) Fu, M.; Tamarat, P.; Trebbia, J. B.; Bodnarchuk, M. I.; Kovalenko, M. V.; Even, J.; Lounis, B. Unraveling Exciton–Phonon Coupling in Individual FAPbI₃ Nanocrystals Emitting near-Infrared Single Photons. *Nat. Commun.* **2018**, *9*, 3318.
- (46) Ithurria, S.; Tessier, M. D.; Mahler, B.; Lobo, R. P. S. M.; Dubertret, B.; Efros, A. L. Colloidal Nanoplatelets with Two-Dimensional Electronic Structure. *Nat. Mater.* **2011**, *10*, 936–941.
- (47) Hinterding, S. O. M.; Salzmann, B. B. V.; Vonk, S. J. W.; Vanmaekelbergh, D.; Weckhuysen, B. M.; Hutter, E. M.; Rabouw, F. T. Single Trap States in Single CdSe Nanoplatelets. *ACS Nano* **2021**, *15*, 7216–7225.
- (48) Feng, D.; Yakovlev, D. R.; Pavlov, V. V.; Rodina, A. V.; Shornikova, E. V.; Mund, J.; Bayer, M. Dynamic Evolution from Negative to Positive Photocharging in Colloidal CdS Quantum Dots. *Nano Lett.* **2017**, *17*, 2844–2851.
- (49) Feng, D.; Yakovlev, D. R.; Dubertret, B.; Bayer, M. Charge Separation Dynamics in CdSe/CdS Core/Shell Nanoplatelets Addressed by Coherent Electron Spin Precession. *ACS Nano* **2020**, *14*, 7237–7244.
- (50) Galland, C.; Ghosh, Y.; Steinbrück, A.; Sykora, M.; Hollingsworth, J. A.; Klimov, V. I.; Htoon, H. Two Types of Luminescence Blinking Revealed by Spectroelectrochemistry of Single Quantum Dots. *Nature* **2011**, *479*, 203–207.
- (51) Rossinelli, A. A.; Rojo, H.; Mule, A. S.; Aellen, M.; Cocina, A.; De Leo, E.; Schäublin, R.; Norris, D. J. Compositional Grading for Efficient and Narrowband Emission in CdSe-Based Core/Shell Nanoplatelets. *Chem. Mater.* **2019**, *31*, 9567–9578.

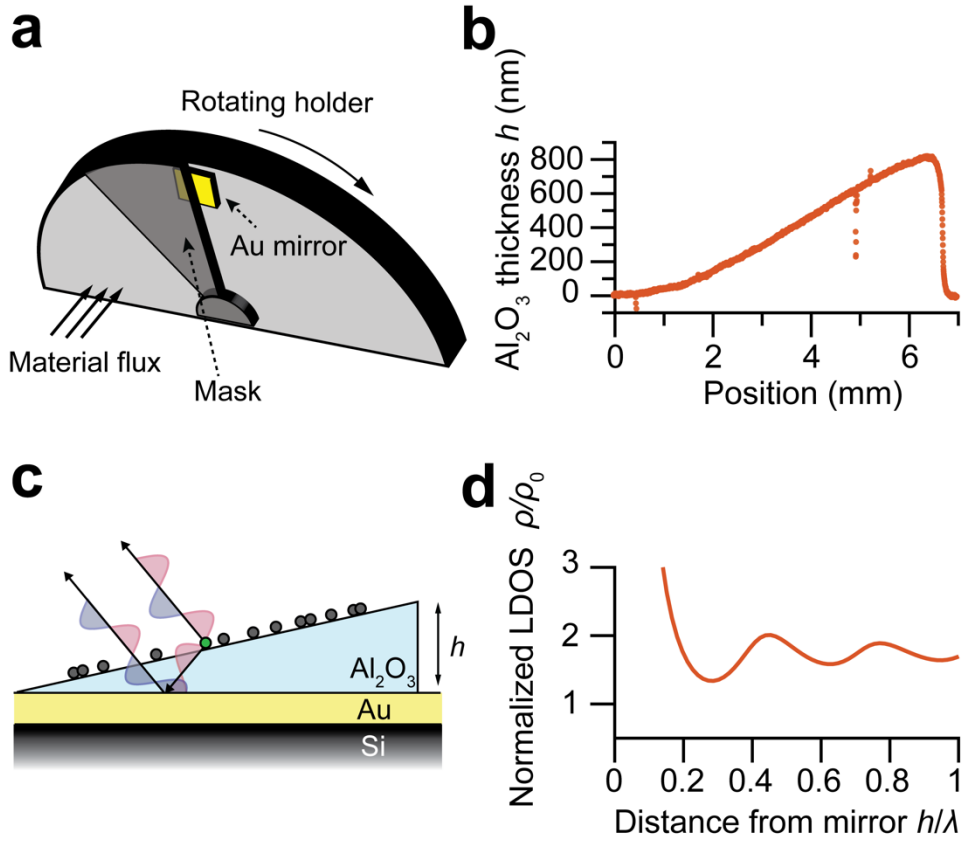


Figure 1. (a) Sketch of procedure for fabricating nanophotonic structures with controlled LDOS. A Au-coated Si substrate is gradually exposed to Al_2O_3 flux by rotating the sample relative to a shadow mask in a reactive sputterer. (b) Thickness profile of the Al_2O_3 ramp measured by profilometry. The dips at horizontal positions 0.5 and 5 mm are due to etch marks on the Si substrate. (c) Sketch of our structure: self-interference between direct and reflected emission at each position along the wedge affects the LDOS. (d) Calculated normalized LDOS, ρ_r , as a function of the wavelength-normalized distance h from a mirror for an isotropic electric-dipole emitter radiating at $\lambda = 535$ nm.

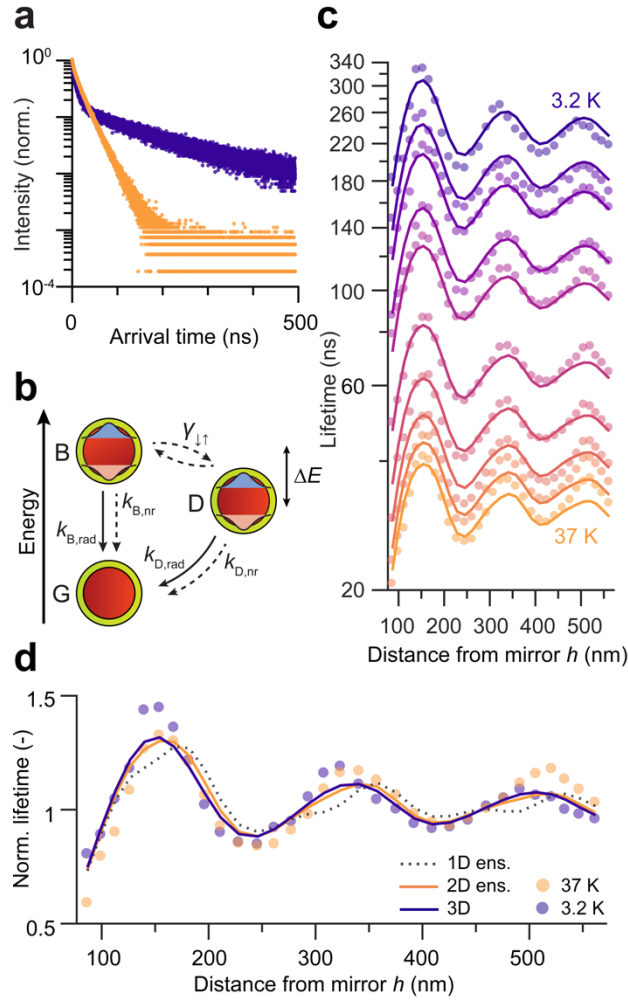


Figure 2. Temperature and LDOS dependency of the long decay component in the low-temperature fine-structure dynamics of CdSe/ZnS core/shell cQDs. (a) PL decay at 3.2 K (blue) and 37 K (orange) recorded at the same distance (230 nm) from the reflector. (b) The model of exciton fine-structure dynamics considered: G, B, and D are the cQD ground state, bright exciton, and dark exciton, respectively. Radiative (nonradiative) transitions are depicted as solid (dashed) arrows. (c) Experimental dependence of the long lifetime component on temperature and distance from the mirror (solid dots). Data are shown for 3.2, 5.2, 7, 10, 12, 17, 22, 27, 32, and 37 K. The solid lines represent the fitted LDOS-temperature model to the data. (d) Dependence of the long lifetime component on the distance from the reflector at temperatures of 3.2 (blue) and 37 K (orange), normalized to the average lifetime values between 300 and 450 nm. The dotted gray, solid orange, and solid blue lines are the normalized ensemble-weighted lifetimes for an ensemble of randomly oriented 1-, 2-, and 3-dimensional electric-dipole emitters, respectively.

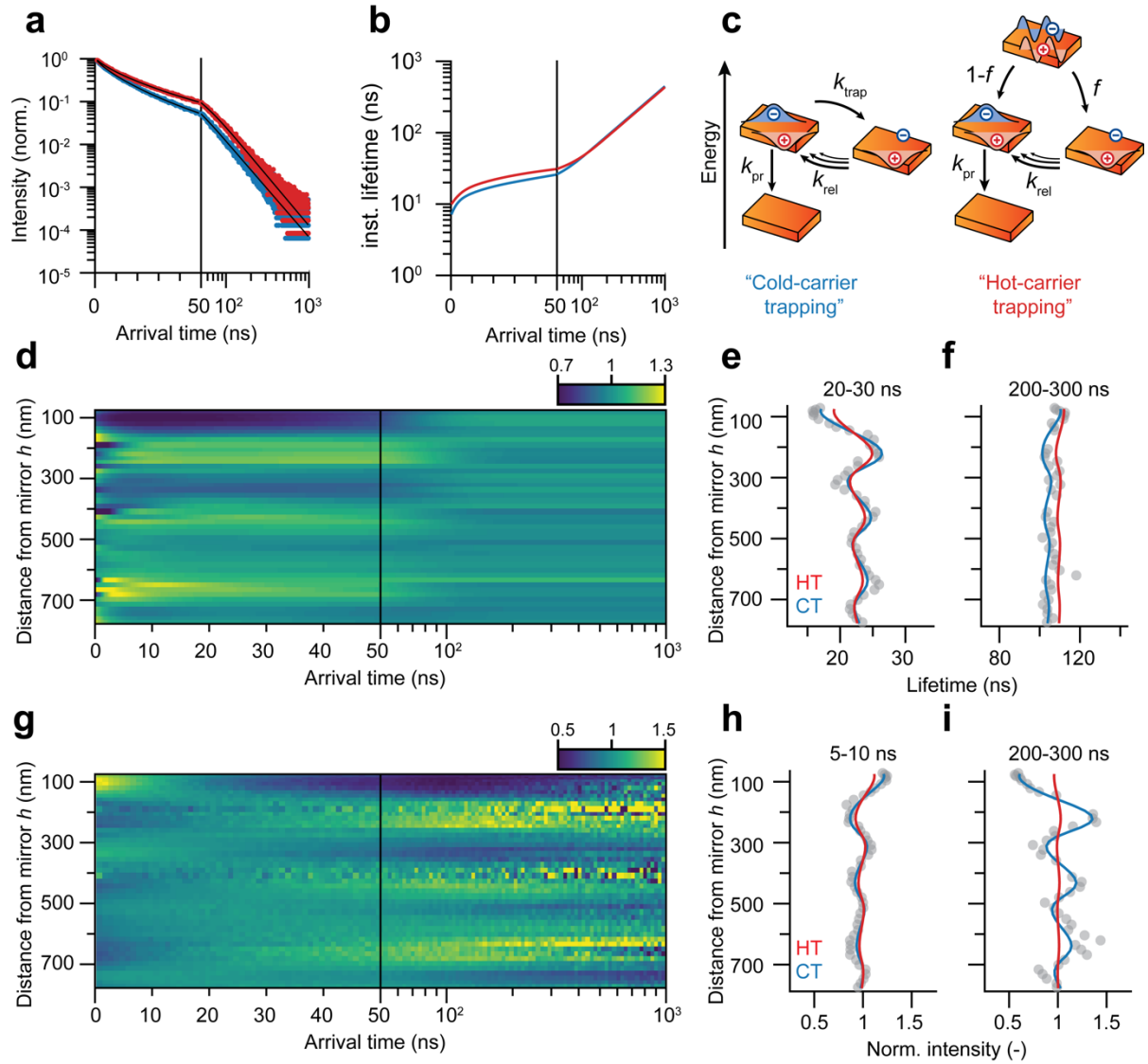


Figure 3: Determining the delayed-emission mechanism in CdSe/Cd_xZn_{1-x}S core/shell NPLs at room temperature. (a) PL decay trace at two distances h from the mirror: 326 (blue) and 448 nm (red). Solid lines are fits to the data. (b) Instantaneous lifetime, calculated from the curves fit to the PL decay in panel a. (c) Cold-trapping (CT) model: “hot” photogenerated carriers relax first to the lowest exciton state. Prompt radiative recombination with rate k_{pr} and carrier trapping with rate k_{trap} then compete. Hot-trapping (HT) model: “hot” photogenerated carriers decay either to the lowest exciton state or directly into a trap state, yielding initial populations of $1 - f$ and f in the lowest exciton and trap states, respectively. In both models, detrapping occurs with a distribution of release rates k_{rel} . (d) Instantaneous lifetime normalized by its mean value at each photon arrival time. (e,f) Instantaneous lifetime as a function of h , averaged from 20 to 30 ns and 200 to 300 ns, respectively. Solid lines are fits to CT and HT models. (g) PL decay curves as a function of h . At each h , the PL decay is first background-

subtracted and normalized to the total counts at that h . Next, the intensity at a particular t is further normalized to the mean intensity at that t . (h,i) Normalized intensity averaged from 5 to 10 ns and from 200 to 300 ns, respectively. Solid lines are fits to the CT and HT models. In panels a, b, d, and g, the time axis is linear between 0–50 ns and logarithmic between 50–1000 ns.